The Developmental Basis of Fingerprint Pattern Formation and Variation

Mathematical Appendix: Finger Ridge Patterning Models & Simulations

Developing a Computational Turing Reaction-Diffusion Model

The initial framework for the reaction-diffusion computational model is based on the human fingerprint pattern being defined by primary ridges whose formation is marked by high levels of EDAR/WNT signaling, where proliferative downgrowth of the epithelium follows. In particular, EDAR tunes activator function and proxies for diffusible epithelial WNT as in other systems[1], with the observations in Figure 4 of the main text highlighting that EDAR controls ridge patterning in the manner of a Turing activator, with stripes becoming spots given the ablation of EDAR signaling. BMP induces an inhibitory effect and is co-localized with EDAR in the fingerprint ridges (Figures 1, 2, 5), analogously to EDAR/WNT and BMP signaling in the early stages of hair follicle formation. In addition, the perception of BMP signal, as indicated by pSMAD1/5 is more extensive around the ridges compared to LEF1, which is promoted by, and a partial readout of, WNT signaling (Figures 1, 5). Finally, as detailed in the main text and supported by its Figures 1C&D, the primary ridge pattern is essentially fixed as it is laid out, with no observed response to digit growth, and thus there is no need to consider additional complications, such as domain growth, in the computational simulations.

The computational framework that models the components highlighted in the previous paragraph is that of a diffusible activator and a diffusible inhibitor, as simple representations of EDAR/WNT and BMP respectively, with EDAR/WNT signaling interpreted as a precursor to, and driver for, the cell proliferation and the subsequent morphological changes that induces ridges. Thus in turn we take the model activator predictions for EDAR/WNT as proxies for ridge formation in mouse and human. Furthermore, the extended spread of pSMAD1/5 entails we take the diffusible inhibitor to have a longer range of signaling, and thus a larger diffusion coefficient, than the activator. That activator signal, as represented by WNT/EDAR and also by LEF1, and the inhibitor signal co-localize requires that we take pure, rather than cross, activator-inhibitor kinetics, whereby the activator promotes production of both itself and the inhibitor while the inhibitor downregulates itself and the activator. We use a common example of such kinetics, as proposed by Gierer and Meinhardt[2], adjusted to ensure activator saturation at high activation levels to limit any prospective high values of the activator[3].

Thus, after a suitable non-dimensionalization, we use the model

$$\frac{\partial u}{\partial t} = r\left(a + \frac{u^2}{v(1+Ku^2)}\right) - \mu u + \nabla^2 u, \tag{1}$$

$$\frac{\partial v}{\partial t} = u^2 - \nu v + D\nabla^2 v \tag{2}$$

for activator-inhibitor signaling. Here, the parameters $\mu > 0$ and $\nu > 0$ represent removal (via degradation or otherwise) of activator and inhibitor respectively, $D > 1$ is the ratio of the inhibitor's diffusion coefficient to that of the activator, and r controls a timescale of activator production, which has a basal production rate $ra > 0$. The term $u^2/(v(1 + Ku^2))$ corresponds to the activator's self-activation, which is inhibited by v and, in an extension of the original Gierer-Meinhardt models[2], saturates at high activator levels, as governed by the parameter $K > 0$ [3]. We take $K \ll 1$ so that the model is a small perturbation of a Gierer-Meinhardt system unless the activator level is high, which also ensures there is a unique steady state (see below). This reaction scheme is summarized in Figure Ax1A. The associated reaction-diffusion equations need to be supplemented with initial and boundary

conditions, which will differ between the models of mouse transverse digit ridge patterning and human primary ridge formation, as detailed below.

1.1 A signaling model that proxies for mouse transverse digit ridge formation

We firstly test the proposed reaction-diffusion system by examining whether its activator, interpreted as a proxy for transverse ridge location, can reproduce murine digit ridge patterning, including the impact of the signaling perturbations considered in the main text.

We represent the geometry of the mouse digit, where the transverse ridges form, by a hemicylindrical segment of cross sectional radius R and height $L = 3R$, that is

$$\Omega := \{(x, y, z) | x^2 + y^2 = R^2, y > 0, 0 \leq z \leq L = 3R\}. \quad (3)$$

As we have no initiation sites within the domain, we take the initial conditions to be

$$u = u^*, v = v^*, \quad (4)$$

where $(u^*,\ v^*)$ constitutes the unique homogeneous steady state of the model, which ensures patterning does not initiate within the interior of the domain.

As the transverse digits initiate distally we use a pattern-initiating boundary condition on the distal boundary $z = L$. There are many potential choices for such boundary conditions, though the form of the pattern are insensitive to the boundary condition details, and, thus, we use

$$u = 0,\ \boldsymbol{n} \cdot \nabla v = 0,\ (x, y, z) \in \partial\Omega_T = \Omega \cap \{z = L\}, \quad (5)$$

whereby the Dirichlet condition $u = 0$ forces the activator away from its homogeneous steady state at the boundary, thus initiating pattern. In contrast, we use Neumann conditions, with $\boldsymbol{n}$ denoting the outward unit normal, for the other boundaries,

$$\boldsymbol{n} \cdot \nabla u = 0,\ \boldsymbol{n} \cdot \nabla v = 0,\ (x, y, z) \in \partial\Omega_O = \Omega \cap \{z = 0 \cup (x, y) = \pm(R, 0)\}, \quad (6)$$

which are compatible with the homogeneous steady state of the system and thus do not initiate patterning.

Simulations for a reference set of parameters are presented in Figure Ax1B-E at a selection of times. These show that the model predicts the distal initiation of pattern at the top of the domain, with a propagating wave of stripes, generating a final, steady state striped pattern of activator signaling and thus transverse ridges at sufficiently large time, as highlighted by plot Ax1E. Ablation of EDAR signaling is modelled by a reduction in the production of activator due to loss of the upregulation of WNT by EDAR[1], while high copy number lines of EDAR are modelled with an increase in this upregulation, so that the parameter r is respectively decreased and increased for these two perturbations. The modeling predictions are shown in Figure Ax1F-J, where a sufficient loss of EDAR function is predicted to induce a pattern of spots as shown in Figure Ax1F, consistent with Figure 4. Furthermore, enhanced EDAR signaling is predicted to induce a larger wavelength of thicker ridges, as seen by comparing Figure Ax1H and Ax1I, consistent with Figure 4.

We proceed to consider the impact of the BMP signal transduction inhibitor LDN193189, which we model by enhancing the removal of the inhibitor signal via increasing the parameter ν, as summarized in Figure Ax1A. The model predicts that inhibiting the BMP signal in this manner does not change the wavelength of the activator and thus the ridges and generates an increase in activator stripe thickness,

with a predicted concomitant increase in ridge thickness, as can be seen by comparing Figure Ax1M to Ax1N, which is consistent with the observations of Figure 5. Thus this simple model of signaling interactions captures all the behaviours observed in perturbing the signaling regulation of murine transverse ridge formation, as summarized in Figure 5 of the main text. Furthermore, since murine transverse ridges represent the closest structures to human primary fingerprint ridges[4], we proceed to consider this patterning framework to qualitatively model the formation of human fingerprints.

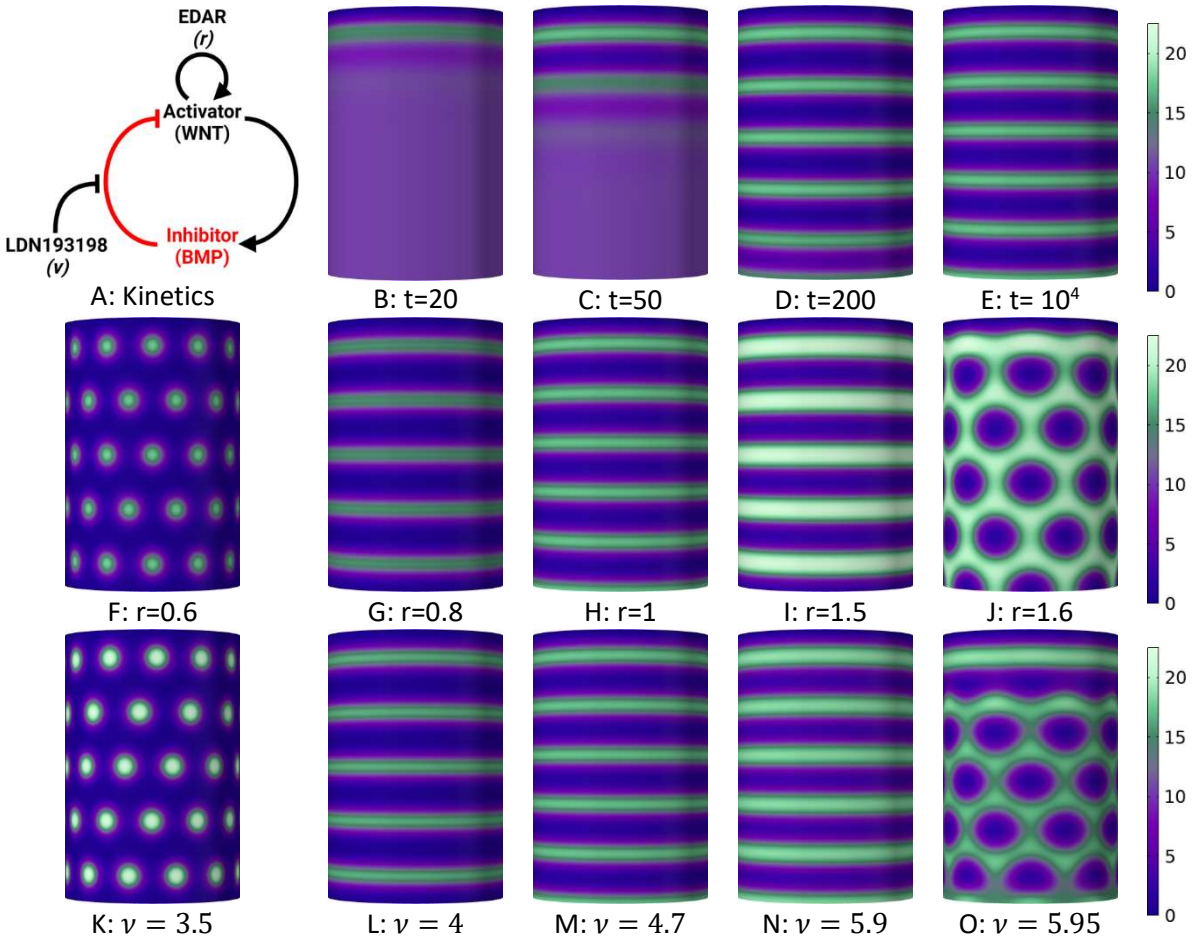

Figure Ax1: A signaling model that proxies for mouse transverse ridges. (A) The activator inhibitor interactions, with the impact of EDAR perturbations on activator production (r) and LDN193198 on the inhibitor (v). (B-O) Stripe formation on the hemicylinder: Plots of u from simulations of (1)-(2) with homogeneous initial data (4) on the surface Ω of (3), with the pattern initiating boundary conditions (5) on the top boundary $\partial\Omega_T$, and Neumann boundary conditions (6) for the other three boundaries, $\partial\Omega_0$, with common parameters $L = 100 = 3R$, $K = a = 0.001$, $D = 180$, and $\mu = 0.4$. (B-E) Stripe formation with reference parameters $r = 1$, $v = 4.7$, with the panels show different simulation times t . (F-J) Increasing Activator Production (r). With $v = 4.7$, the panels show essentially the final pattern at $t = 10000$, with transitions from Spots → Stripes → Holes as r increases, with further increases in r leading to the loss of patterning. (K-O) Increasing Inhibitor Removal (v). With $r = 1$, the panels show essentially the final pattern at $t = 10000$, with transitions from Spots → Stripes → Holes, as v increases, with further increases in v leading to the loss of patterning.

1.2 A signaling model that proxies for human primary ridge fingerprint formation

In addition to Eqns (1)-(2) summarising this signaling of Figure Ax1A, model construction requires initial and boundary conditions and these are motivated by the observations of patterning initiation sites for primary ridges in human. In particular, for the fingertip, the first primary ridges can be observed to emerge on the central part of the distal volar pad around week 13 in human, with further patterning initiation adjacent to the nail bed and dorsal/ventral boundary at the tip of the digit, as highlighted by Figures 6A, S4A, S7B and S7C. Additional initiation is observed adjacent to the interphalangeal crease (Figure S7). In particular, while ridge formation cannot occur within this crease, which is consistent with its mechanical microenvironment, patterning nonetheless can initiate immediately adjacent to, and parallel with, the crease though often later than fingertip central pad initiation. Thus we develop a model for EDAR/WNT signaling, interpreted as a proxy for human primary ridge fingerprint formation at the fingertip by considering a domain faithful to the human fingertip ventral pad with the signaling of Figure Ax1A via Eqns (1)-(2). This system is closed via initial and boundary conditions representing the timing and location of primary ridge pattern initiation sites.

1.2.1 Fingertip geometry For the fingertip ventral pad geometry we take a hemicylinder of height L and radius $R = 2L/5$, topped with a spherical shell quadrant of radius R , as depicted in Figure Ax2A &2B with Ω relabelled to now represent this domain. The panels also highlight the labeling of different regions that partition $\partial\Omega$, the boundary of Ω, with $\partial\Omega_B$ denoting the bottom boundary of the hemicylinder, which represents the edge of the interphalangeal crease and is a boundary patterning initiation site. As a representation of the nail bed edges on the boundary of the distal fingertip, which is a second boundary initiation site, we take the union (combination) of $\partial\Omega_T$ – the upper boundary of the spherical shell and the nail bed – and $\partial\Omega_{S1}$, the lateral side of the nail bed, so that the nail bed initiation site is $\partial\Omega_{NB} = \partial\Omega_T \cup \partial\Omega_{S1}$. The dorsal-ventral boundary proximal to the nail bed is denoted by the boundary $\partial\Omega_{S2}$ and does not feature as an independent initiation site for the arch, loop, or whorl fingerprint phenotypes.

1.2.2 Initial conditions and initiation sites: whorl, loop and arch

To describe initiation sites it is useful to introduce a localized bump function:

$$\Phi(s) = \begin{cases} \exp\left(1 - \frac{1}{1-s^2}\right) & |s| \leq 1, \\ 0 & |s| > 1. \end{cases} \tag{7}$$

Note that for the fingertip the first primary ridges are often observed to emerge on the center of the fingertip volar pad, and are anticipated by elevated EDAR and LEF1, first observed on the proximal slope of the pads with a subsequent spread to the distal tip (Figures 6A & S7). We thus represent patterning initiation on the volar pad of the fingertip via initial conditions of the model with a localized elevation of activator. Differences in the spatial localisation of the initiation are considered since Turing systems are not only inherently sensitive to initial profiles of activator but also because there is clearly a source of variability underlying fingerprint formation, reflected in the individual uniqueness of the patterns ultimately produced.

Whorl Initial Conditions In particular, for a highly localized distal pad initiation site we take the initial condition for the model to be

$$u(0,x,y,z) = u^*(1 + 0.1\Phi(X(x,y,z))), \quad v(0,x,y,z) = v^*, \quad (x,y,z) \in \Omega, \tag{8}$$

where

$$X(x,y,z) = X_W(x,y,z) := 10\left(\left(\frac{x+R}{R}\right)^2 + \left(\frac{y}{R}\right)^2 + \left(\frac{z-0.8L}{R}\right)^2\right)^{1/2}, \quad (9)$$

and u^* and v^* represent the values of activator and inhibitor at the homogeneous steady state. Thus the inhibitor is uniformly at its homogeneous steady state but the activator is locally elevated as plotted in Figure Ax2G in green, where this panel and the others in Figure Ax2 have two virtual lighting sources to emphasize the geometry of the fingertip. Note that Figure Ax2G is labelled as a whorl initial condition since we use it to simulate human primary ridge formation constituting a whorl fingerprint pattern below.

Loop Initial Conditions We can alternatively consider an initiation site on the fingertip with elevated activator but of limited localisation, with activator expression in a region that spreads across the ventral pad, as represented by Eqn (8), where $X(x,y,z)$ is instead given by

$$X(x,y,z) = X_L(x,y,z) := 10\left(\left(\frac{x+R\mathrm{si}\left(\frac{3z}{2L}\right)}{R}\right)^2 + \left(\frac{y-R\cos\left(\frac{3z}{2L}\right)}{R}\right)^2\right)^{1/2} \quad (10)$$

for instance. This initial activator profile is depicted in Figure Ax2L in green and labelled with loop we use this initial condition to simulate human primary ridge formation constituting a loop fingerprint pattern below.

Arch Initial Conditions Finally, for arch like fingerprint simulations we consider the possibility that primary ridges fail to initiate prior to pattern arrival from other initiation sites within the interior of the distal pad and thus the initial condition is simply

$$u(0,x,y,z) = u^*, \quad v(0,x,y,z) = v^*, \quad (x,y,z) \in \Omega. \quad (11)$$

This is depicted in Figure Ax2R by the absence of green, in comparison to Figure Ax2G&2L. This initial condition will not induce patterning on the domain interior and will be used as an initial condition in the simulation of arch fingerprint primary ridge patterns below.

1.2.3 Boundary conditions and initiation sites

Primary ridge initiation is also observed at a number of sites on the boundaries of the fingerprint domain we consider, in particular at the fingertip by the nail bed boundary and adjacent to the interphalangeal crease (Figures 6A and S7). Furthermore, while ridge formation cannot occur within this crease, as consistent with its mechanical microenvironment, patterning nonetheless can initiate immediately adjacent to, and parallel with, the crease though often temporally later than any initiation on the pad (Figure S7). Thus we require boundary conditions that initiate elevated activator levels for primary ridge formation at these loci on the boundary, though with initiation suitably timed among the different initiation sites and we also require boundary conditions that do not initiate pattern.

To ensure the absence of activator and ridge pattern initiation where relevant we use Neumann boundary conditions

$$\mathbf{n} \cdot \nabla u = 0, \quad \mathbf{n} \cdot \nabla v = 0, \quad (12)$$

where $\mathbf{n}$ is the outward unit normal that lies in the tangent plane of the surface, as motivated previously for Eqn (6) of the mouse transverse ridge model. For boundaries where pattern initiation

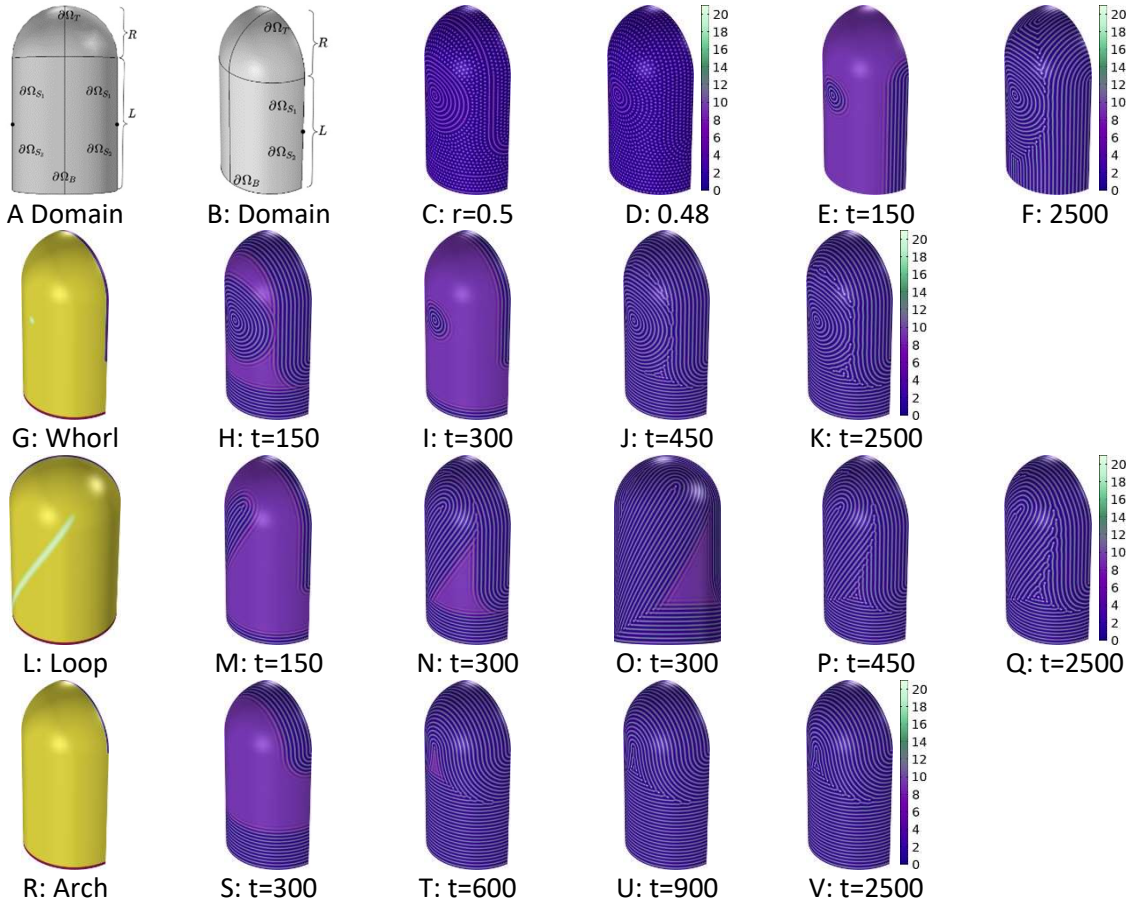

Figure Ax2: A signaling model that proxies for human primary ridge formation (A,B) Domain geometry and boundaries. (G,L,R) The pattern initiation regions for a whorl, loop and arch pattern, with internal initiation regions in green and apical and basal boundary pattern initiation locations in blue and red. The timing of pattern initiation in the latter regions is given by T_a, T_b below, as detailed in the text. (H-K,M-Q,S-V) Predictions for activator levels (according to the color scale on the right) that proxy for human primary ridge formation, from Eqns (1)-(2) at the times t shown in the panel labels, with the common parameters: $L = 600 = 5R/2$, $a = K = 0.001$, $D = 180$, $r = 0.75$, $\mu = 0.4$, and $\nu = 5.5$. (H-K) Simulations of whorl formation using the initiation regions of (G) and timings $T_a = T_b = 50$ for boundary conditions (13) on Ω_T, Ω_{S1} , and Ω_B with Neumann conditions (12) on all other boundaries. (M-Q). Simulations of loop formation using initiation regions of panel (L) and timings $T_a = T_b = 50$ for the boundary conditions (13) on Ω_T, Ω_{S1}, and Ω_B with Neumann conditions (12) on all other boundaries. (S-V) Simulations for arch formation using the initiation regions of (R) and timings $T_a = 100$, $T_b = 0$ for the boundary conditions (13) on Ω_T and Ω_B, with Neumann conditions (12) for all other boundaries. (C-F) Simulation prediction for whorl simulations with: (C,D) the final pattern for reduced values of activator production (r), highlighting a *ridge-dissociation* phenotype; (E,F) boundary initiation sites only on, $\partial\Omega_{S1}$, $\partial\Omega_{S2}$, giving the pattern shown at the labelled times, which exhibits *"ridges off the end"* for the final pattern phenotype.

can occur, a time-dependent boundary condition is needed as such initiation is often later than pattern initiation on the fingertip volar pad. Thus for such boundaries we use

$$(1-A(t))\mathbf{n}\cdot\nabla u + A(t)u = 0, \quad \mathbf{n}\cdot\nabla v = 0, \quad A(t) = \begin{cases} 0, & t < T, \\ \frac{t-T}{100}, & T \le t \le T+100, \\ 1, & t > T, \end{cases} \tag{13}$$

which transitions from the absence of boundary pattern initiation for $t < T$ to the patterning initiating conditions (5) for $t > T + 100$, with a brief interpolation between these conditions. These time-dependent conditions model a later-starting fingertip boundary initiation site. We will use boundary conditions (13) with the parameter $T = T_a$ to represent the condition at nail bed boundary. Similarly, we will use boundary conditions (13) with a parameter $T = T_b$ for the proximal interphalangeal crease boundary, Ω_B.

1.3 Results

We present results for the pattern formation model of EDAR/WNT signaling that is taken to proxy for human primary ridges, Eqns 1, 2 on the domain geometry depicted in Figure Ax2A&2B and the parameter values given in Figure Ax2. A selection of initial and boundary conditions are simulated, representing the spatiotemporal range of initiation sites and timings to consider the formation of whorl, loop, arch and rarer patterns of primary fingerprint ridges.

Whorl For whorls we use the initial condition given by Eqns 8, 9, as illustrated in Figure Ax2G. We have the time-dependent pattern initiation boundary conditions (13) on the nail bed initiation site is $\partial\Omega_{NB} = \partial\Omega_T \cup \partial\Omega_{S1}$ (Figure Ax2A&2B), with pattern initiation at $T = T_a = 50$. Similarly, we have the time-dependent pattern initiation boundary conditions (13) at the interphalangeal crease $\partial\Omega_B$, with the initiation of pattern at $T = T_b = 50$, and Neumann conditions (12) that do not initiate pattern on all other boundaries. The predicted pattern is illustrated in Figure Ax2H-K and illustrates the initiation of three waves at each of the initiation sites in Figure Ax2G. In particular, the predicted activator profiles that proxy primary ridges emerge oriented parallel to boundary with this boundary condition, even though this orientation is not explicitly imposed. Furthermore, the initiated waves spread from the initiation sites with their mutual confluence inducing triradius formation (Figure Ax2J), with the established long term predicted whorl-like pattern given by Figure Ax2K.

Loop Loops have the same boundary conditions as whorls, but with a loop initial condition, given by Eqns 8,10, as illustrated in Figure Ax2L. This extended region of initiation influences where the waves meet, giving rise to a different, and here loop, pattern (Figure Ax2N&2O). Once more the three waves confluence to induce a triradius (Figure Ax2P), with long term persistence of the loop pattern (Figure Ax2P).

Arch For an arch, ridge initiation in the interior of the distal pad fails to occur prior to pattern arrival from other initiation sites, and hence we use the homogeneous initial condition in Eqn 11. Secondly, the pattern characteristics suggest that distal initiation is suppressed or delayed so that a proximally initiating wave propagates sufficiently to allow confluence with the wave spreading from the distal region. Hence we spatially limit the nail bed initiation site and only allow initiation on a distal restriction, $\partial\Omega_T$, of the nail bed-fingertip boundary (Figure Ax2R), and we also temporally delay this initiation with $T = T_a = 100$ in the boundary condition of Eqn (13). In contrast, pattern initiation from the interphalangeal crease – boundary $\partial\Omega_B$ of plots Ax2A&2B – is taken to occur first, at $T = T_b = 0$ in the pattern initiation boundary condition of Eqn (13). The patterning inert, Neumann, boundary

conditions of Eqn 12 are imposed on all other boundaries. The predicted pattern illustrates the initiation of two waves at the initiation sites (Figure Ax2R) and establishment of a predicted arch pattern (Figure Ax2V).

Rarer fingerprint patterns For the predicted EDAR/WNT signaling dynamics to produce a pattern that proxies for the rare *ridge dissociation* fingerprint, we consider the conditions for the whorl fingerprint, but with a reduced value of activator production, as governed by the parameter r . In particular, with a 50% decrease in this parameter the ridges have clearly dissociated (Figure Ax2C), and almost completely dissociated with a small further decrease in r (Figure Ax2D). Similarly, *"ridges off the end"* can be induced by altering the boundary initiation of the whorl-forming phenotype, with boundary pattern initiation no longer at the distal nail bed, but instead along just the dorsal ventral boundary, that is both $\partial\Omega_{S1}$, $\partial\Omega_{S2}$ of Figure Ax2A&2B. The early time evolving pattern and the final time pattern clearly exhibit ridges running perpendicular to the simulated digit distal tip (Figure Ax2E&2F).

Steady State of the Model

We note that spatially homogeneous steady state(s) of Eqn (1), denoted by (u^*, v^*), satisfy $v^* = (u^*)^2/v$ where u^* satisfies the cubic equation,

$$Ku^3 - aK\frac{r}{\mu}u^2 + u - \frac{r(v+a)}{\mu} = 0. \tag{14}$$

The constant term is negative and hence the cubic is negative at $u^* = 0$, and is also positive as $u^* \to \infty$; thus there is always at least one positive real root. Looking for turning points of this equation we find that if $a^2K < 3\mu^2/r^2$, there are no real turning points and hence there is one, and only one, real root, which is positive. Given we have $K \ll 1$ so that the model is close to the original Gierer-Meinhardt model unless there are very large levels of activator, this condition is trivially satisfied for the parameters considered.

Summary

We have shown how experimental investigations demonstrating that mouse transverse ridge formation and human primary ridge formation can be anticipated by cellular signaling enables the development of a computational Turing model with activator-inhibitor kinetics that proxies ridge formation. In particular, the form of the model and that it is a Turing system are motivated from the experimental observations.

A feature of the presented computational model is that the upstream events that generate the heterogeneity of pattern initiation sites is simply imposed via the initial conditions, as a reflection of prior limb and digit development, reflecting the observed constraints on the patterning system. A further aspect of the model is that the boundary conditions are phenomenological, representing the heterogeneous dynamics at the boundary pattern initiation sites. One should not interpret the Neumann and Dirichlet conditions as perfectly reflecting and absorbing physical boundaries in this model since such boundaries to chemical diffusion are incompatible with observation. In particular, reflecting, or absorbing, boundaries are not necessary for Neumann and Dirichlet conditions, which can also be generated for instance by a sharp transition in the cellular response to diffusible signals, as demonstrated by Krause et. al.[5]. Here the boundary conditions also simplify the mechanism of micromechanical prevention of ridge formation in the interphalangeal creases by abbreviating these into an output of altered signaling.

The model demonstrates how signaling dynamics captures the behaviour of all experimental perturbations. It demonstrates how signaling modulation induces spot condensations of elevated activator, as required for consistency with observations that the system is an abridged hair follicle patterning system, while still generating all responses of the labyrinthine activator patterns in mouse perturbation studies. Furthermore, with patterning initiation suitably represented, the model readily demonstrates that the huge variety in human fingertip primary ridges is consistent with limited changes in the location and timings of a small number of activator initiation sites, including rare fingerprint pattern types.

References

1. Zhang, Y., Tomann, P., Andl, T., Gallant, N.M., Huelsken, J., Jerchow, B., Birchmeier, W., Paus, R., Piccolo, S., Mikkola, M.L., et al. (2009). Reciprocal requirements for EDA/EDAR/NF-kappaB and Wnt/beta-catenin signaling pathways in hair follicle induction. Dev Cell *17*, 49-61. S1534-5807(09)00213-5 [pii]

10.1016/j.devcel.2009.05.011.
2. Gierer, A., and Meinhardt, H. (1972). A theory of biological pattern formation. Biological Cybernetics *12*, 30-39.
3. Kolokolnikov, T., Sun, W., Ward, M., and Wei, J. (2006). The stability of a stripe for the Gierer–Meinhardt model and the effect of saturation. SIAM Journal on Applied Dynamical Systems *5*, 313-363.
4. Li, J., Glover, J.D., Zhang, H., Peng, M., Tan, J., Mallick, C.B., Hou, D., Yang, Y., Wu, S., Liu, Y., et al. (2022). Limb development genes underlie variation in human fingerprint patterns. Cell *185*, 95-112 e118. 10.1016/j.cell.2021.12.008.
5. Krause, A.L., Klika, V., Maini, P.K., Headon, D., and Gaffney, E.A. (2021). Isolating Patterns in Open Reaction-Diffusion Systems. Bull Math Biol *83*, 82. 10.1007/s11538-021-00913-4.